

## Optical and field emission properties in different nanostructures of ZnO

Jai Singh<sup>a\*</sup>, P. Kumar<sup>a</sup>, D. J. Late<sup>b</sup>, Trilok Singh<sup>c</sup>, M. A. More<sup>b</sup>, D. S. Joag<sup>b</sup>, R. S. Tiwari<sup>a</sup>, K.S. Hui<sup>d</sup>, K.N. Hui<sup>e</sup>, O.N. Srivastava<sup>a</sup>

<sup>a</sup>*DST Unit for Nanoscience, Dept of Physics, Banaras Hindu University, Varanasi, India- 221005.*

<sup>b</sup>*Department of Physics, University of Pune, Pune, India-411007*

<sup>c</sup>*Thin Film Laboratory, Department of Physics, Indian Institute of Technology Delhi, Hauz Khas, New Delhi-110016, India*

<sup>d</sup>*Department of Systems Engineering and Engineering Management, City University of Hong Kong, Hong Kong*

<sup>e</sup>*School of Materials Science and Engineering, Pusan National University, Republic of Korea*

ZnO nanostructures with different morphologies e.g. nanotetrapods, nanorods, nanocombs and nanoaeroplanes has been fabricated by evaporation of pure zinc powder without catalysts in the temperature range of 400–900 °C. The structures and properties of obtained products were examined using scanning electron microscopy, transmission electron microscopy, selected area electron diffraction, X-ray diffraction, room temperature photoluminescence and field emission. Photoluminescence spectra showed an ultraviolet-green emission and strong orange–red emission peaks at room temperature. The field emission studies of the as grown nanocombs revealed that threshold field, required to draw a current density of  $\sim 1.0 \mu\text{A}/\text{cm}^2$  is  $\sim 1.4 \text{ V}/\mu\text{m}$ . An emission current density of  $\sim 9.05 \mu\text{A}/\text{cm}^2$  has been drawn from nanocombs at an applied electric field of  $\sim 1.92 \text{ V}/\mu\text{m}$ . The field enhancement factor found to be  $\sim 8050$ , indicating that the electron emission from nanometric dimension of the emitter. Such, ZnO nanostructures are likely to be candidates as building blocks for constructing photonic and flat panel display.

(Received January 9, 2012; Accepted April 5, 2012)

*Keyword:* Field emission; Nanowires; Nanocombs; Current stability; ZnO.

### 1. Introduction

In the present scenario, metal oxides and their nanostructures have emerged as vital class of materials with a prosperous spectrum of properties and immense potential for device applications. This includes transparent electrodes, high-electron mobility transistors, gas sensors, photovoltaic and photonic devices and hydrogen storage applications. In addition, wide-band gap oxide semiconductors have come to the forefront in the past decade because of an increasing need for short wavelength photonic devices, high-power, high-frequency electronic devices [1]. While many efforts have focused on  $\text{TiO}_2$ ,  $\text{CuO}_2$  and  $\text{SnO}_2$  other wide band gap materials in particular ZnO is now emerging as potential materials for the above applications. Zinc oxide (ZnO) a wide-band-gap II-VI semiconductor has the direct band gap of about  $\sim 3.37 \text{ eV}$  at room temperature with high excitonic binding energy ( $\sim 60 \text{ meV}$ ), is well-recognized functional material suitable for various applications such as optoelectronic, the solar cell and so on [2-5]. ZnO is also a promising material in nanotechnology applications, for example in electronics, field emission and hydrogen storage. In the past few years, extensive efforts have been paid on the synthesis and to understand the growth parameters ZnO nanostructures such as nanorods, nanowires, nanocombs, nanotetrapods, nanobelts and nanorings due to their importance both in scientific and technological aspect. Nanostructured ZnO have been synthesized by various methods, such as chemical vapour deposition [6], laser ablation [5], molecular beam epitaxy [5] or a simple method just by heating

Zn powders with or without catalyst [8, 9]. The combined thermal evaporation and vapor transport method is a promising and most frequently used due technique to the high yield, easy scalability and low cost [9-16]. It has been shown that ZnO nanomaterials (e.g. nanorods, nanowires, nanocombs, nanotetrapods, nanobelts and nanorings ) can be obtained by varying the deposition conditions in relatively ease way. However, precise control for the yield of desired ZnO nanomaterials synthesis remains a big challenge. Thermal evaporation technique is a powerful technique for the synthesis of various ZnO nanostructured. Some delicate hierarchical ZnO nanostructures with 2-, 4- and 6-fold symmetries have also been obtained [17-18]. Wang and co-workers have successfully fabricated a variety of ZnO nanostructures by high-temperature ( $\geq 950$  °C) vapour transport and condensation (VTC) process using ZnO powder as the source material [13]. The structure of ZnO can be described as a number of alternating planes composed of tetrahedrally coordinated  $O^{2-}$  and  $Zn^{2+}$  ions stacked along the *c*-axis. The oppositely charged ions produce positively charged (00.1) Zn-polar and negatively charged (00.1) O-polar surfaces, resulting in a normal dipole moment and spontaneous polarization along the *c*-axis [19]. Due to its hexagonal wurtzite structure, in which the three fastest growth directions,  $\langle 0\ 0\ 1 \rangle$ ,  $\langle 0\ 1\ 0 \rangle$  and  $\langle 1\ 0\ 0 \rangle$ , and its polar crystal surfaces exist, ZnO exhibits a large family of nanostructures [20]. In addition to the conventional nanowire and nanobelt structures, a diverse group of novel ZnO nanostructures has been discovered recently, such as nanocages [21], nanorings [22], nanohelices/nanosprings [23], nanobows [23], nanodiscs [24], nanotetrapods and Nanocombs [25,26] etc. These novel nanostructures not only indicated that ZnO contains probably the richest family of nanostructures among all materials, in both structures and properties, but also provided valuable models in understanding crystal growth mechanisms in nanometre scale and exhibited high potential for fabricating novel nanoelectronic and optical devices with enhanced performance. Among all these different structures, ZnO comb like structures are of interest for nanocantilever arrays, laser arrays nanocomb biosensors and gratings [29-31] etc.

In the previous reports, we have succeeded in the growth of large quantities of ZnO nanorods, nanotetrapods, nanoparticles and nanoflowers by thermal evaporation technique [8-10]. Here, we report the results of the synthesis and properties of various ZnO morphological structures grown in a tube furnace via the thermal evaporation and vapor transport method. Novel ZnO nanostructures have been fabricated such as nanocombs, nanorods, nanotetrapods-like networks and nanoaeroplanes. Photoluminescence from the as synthesized ZnO nanorods and nanocombs have also been presented. These ZnO nanostructures can be utilized for electronic and photonic devices, as well as for biosensors for futuristic applications due to their special morphology.

## 2. Preparation of ZnO nanostructure

Different ZnO nanostructures have been synthesized by thermal evaporation of Zn powder at different temperature using different gas flow rates. Zn powder (Thomas Baker ~325 meshes, 99.9%) was thermally evaporated at  $\sim 900$ -700 °C with different oxygen flow rates. No metal catalysts or special substrate and vacuum system were used in the present investigation. The whole setup was then placed into a horizontal tube furnace. The ZnO, which was evaporated under simultaneous flow of  $O_2$  and Ar ambient was deposited in a silica tube (diameter 3 cm, length 100 cm), which was put in a two-zone furnace. After  $\sim 10$ –15 minutes of evaporation, the furnace was cooled down to room temperature. The temperature gradient along the quartz tube was measured before synthesis, so that the growth temperature of different nanostructures could be determined. In different temperature region white-cotton like products get formed on the inner wall of the silica tube and on alumina boat [8-10]. The obtained nanostructures were examined using scanning electron microscopy (SEM Philips XL-20, ESEM Technai Quanta 200 attached with EDAX), transmission electron microscopy (TEM Philips CM-12 and HR-TEM Technai 20 G<sup>2</sup>), selected area electron diffraction (SAED), and X-ray diffractometer (XRD Philips PW-1710 and X'Pert PRO PANalytical). The photoluminescence (PL) measurement was carried out at room temperature with a He–Cd laser excited at 325 nm.

### 3. Results and discussion

In previous work, ZnO nanotetrapods, nanoparticles, nanoflowers, aligned nanorods have been synthesized by the thermal evaporation method without any catalyst and additives [8-10]. It has been found that novel ZnO nanostructures such as nanocombs, nanorods, nanoaeroplanes, nanotetrapod-like networks and nanocages could be obtained by varying the experimental conditions. The as grown all flux (white cotton like product) was subjected to XRD characterization for the identification of the gross structure. X'Pert PRO (PAN analytical) X-ray diffraction ( $\text{CuK}\alpha$ , 35 KV, 30 mA) was employed for structural characterization. The diffractometer was calibrated with pure Si powder ( $d_{111} = 3.1353 \text{ \AA}$ ). X-ray diffraction (XRD) confirmed that all nanostructures have hexagonal (Wurtzite) ZnO structure with lattice parameters of  $a = 3.249 \pm 0.005 \text{ \AA}$  and  $c = 5.208 \pm 0.004 \text{ \AA}$  (JCPDS file no. 36-1451) and the corresponding pattern is shown of ZnO sample in Fig. 1. No diffraction peak from Zn or other impurity phases is found in any samples, confirming that the products are single phased pure ZnO.

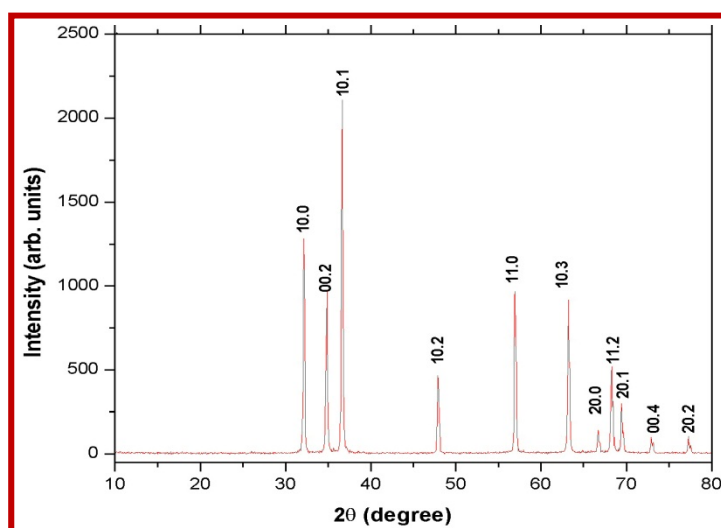


Fig. 1 XRD pattern of as-grown ZnO sample.

#### 3.1 Investigation of ZnO Nanocombs

ZnO nanocombs can be obtained in the condition of 750~800 sccm (standard cubic centimeters per minute) total gas flow rate and ~ 35% fraction of oxygen in the fabrication through pure zinc powder evaporation without catalyst at temperature of 800~900 °C. The as-synthesized ZnO sample was analyzed by scanning electron microscopy (SEM). Figures 2 (a-b) shows a representative SEM image of the nanocomb structure. The image shows that all the ZnO nanocomb are composed of a base (stem) with one-dimensional ZnO nanorod arrays grown perpendicularly on one side over the length span of the stem. The formation of ZnO nanocombs at the site near the source material is in very good agreement with the previous reports [32]. The variation in the width of the stem of the nanocomb has been found to range from ~3.5  $\mu\text{m}$  to ~5  $\mu\text{m}$  and length of the nanocomb is up to several tens of microns. The teeth of combs are normal to comb-stems and nearly evenly distributed along one side of the comb-stem, with an average diameter ranging from ~65 to 125 nm and length ~5 to 6  $\mu\text{m}$ . High magnification SEM image Figure 2(b) shows aligned and nearly evenly spaced nanoteeth with almost constant diameter and spacing between the teeth.

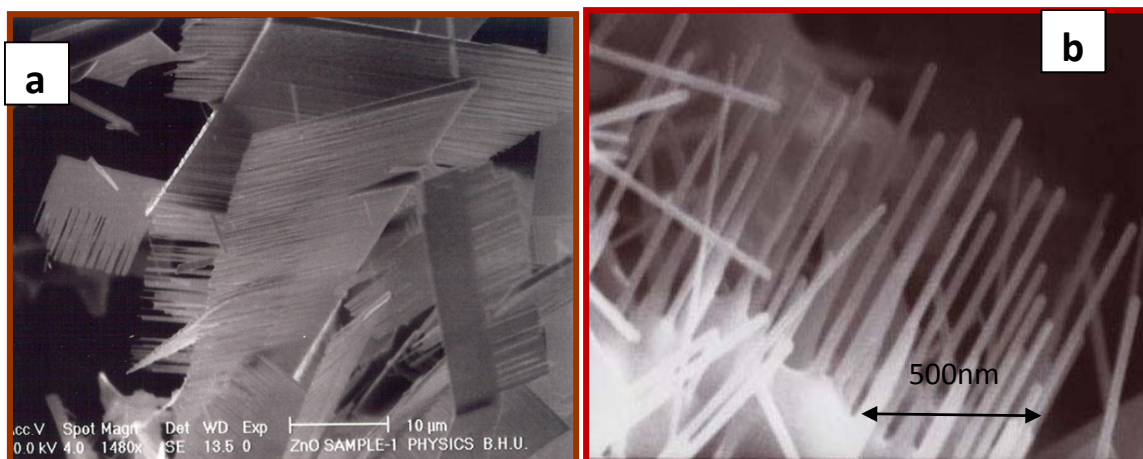


Fig. 2 (a & b) A low magnification and high magnification SEM image of the ZnO nanocombs, respectively.

For further characterization of nanocomb, transmission electron microscopy has been employed (Tecnai 20 G<sup>2</sup> FEI). TEM image of the comb structure is shown in Figure 3. Selected area electron diffraction as shows in inset of Figure 3 reveals that the comb-stems have grown along [01.0] and the nanoteeth have grown along [00.1]. Characterization by XRD, SEM, TEM and SAED verified that no Zn particle was observed at the tips of the synthesized ZnO nanocombs. This indicates that the synthesized ZnO nanostructure were self assembled through a vapor-solid (VS) mechanism, instead of the vapor liquid solid (VLS) mechanism. Due to the intrinsic properties, it is easy for wurtzite ZnO to grow into anisotropic one-dimensional nanostructure. The growth habit of crystals is mainly determined by the internal structure of a given crystal and is also affected by external conditions such as temperature, supersaturation, pressure etc. The growth habit of the crystal reflects the difference in relative growth rates of different crystal faces.

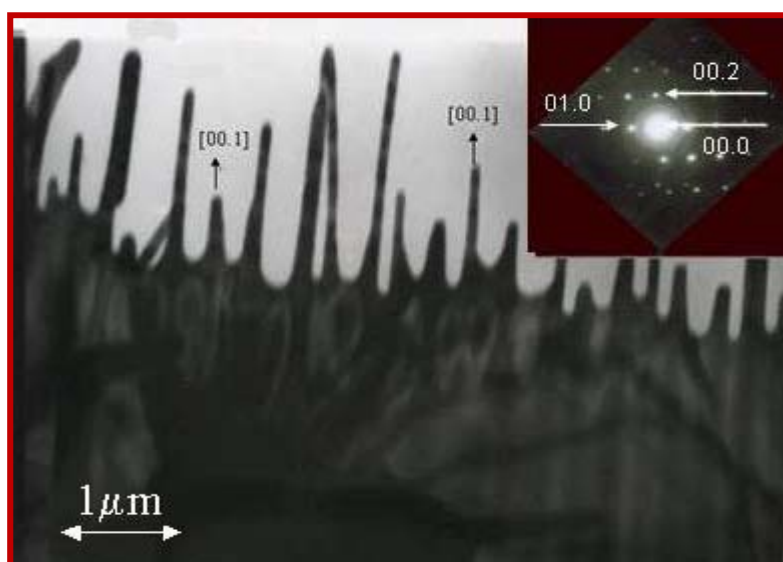


Fig. 3 TEM image of an individual ZnO nanocomb and in the inset SAED pattern taken from teeth. This shows the growth of the teeth along [00.1].

In the present investigation, the nanocomb structures have been fabricated by control of the vapor phase transport. The growth process of the self-assembled nanostructures can be thought to be comprised of two steps. Initially fast growth occurs along [01.0] direction forming the comb-stems. In the beginning slower growth along [00.1] direction on (00.1) surface occurs till the stems acquires a critical thickness. After some critical thickness of the stem, formation of ‘teeth’ along [00.1] direction takes place. The nanocomb formation depends on initial growth condition; low

concentration of oxygen and somewhat higher temperature appears to be conducive for the fast growth along  $[01.0]$  and  $[11.0]$  directions. It may be pointed out that the  $(01.0)$  and  $(11.0)$  surfaces are non-polar and will form based on classical theory of crystal growth [27]. The stem formation will take place through nucleation of embryo at high supersaturation of a size greater than critical size. This embryo further grows through the addition of atoms/molecules and a micro base like stem gets developed. We propose that the actual growth leading to the formation of nanostructures takes place through a second growth process where condensation of oxygen vacancies leads to the formation of Zn rich  $\text{ZnO}_x$  regions. Schematic elucidating the formation of nanocomb in terms of the proposed mechanism is shown in Fig. 4. In the upper part of the picture nearly ordered  $\text{ZnO}_x$  regions on the stem have been outlined. In the lower part the growth of the teeth (nanorods) leading to the formation of complete ZnO nanocomb has been outlined.

### 3.2. Formation of nanorods

By varying experimental conditions, large embodying ZnO nanorods could be obtained. A representative SEM image of the ZnO nanorods fabricated on alumina boat at  $\sim 900^\circ\text{C}$  is shown in Fig.5. As shown in the image, the ZnO nanorods are well uniform on a large scale. The inset in Fig. 5 is a high magnification SEM image, which shows that the nanorods have hexagonal tip with the diameter of about 150 to 450 nm. The possible growth mechanism of the nanorod is vapor-solid (VS) mechanism, because no metal catalysts are used, in whole evaporation procedure. So the growth is different from the traditional vapor-liquid-solid (VLS) mechanism. But the mechanism of growth of ZnO is still an open question and needs more study. Many proposed mechanism have been developed such as constraint of the pores in either mesoporous silicon or porous anodic alumina, Vander walls interaction, effects of DC bias and so on. In this work, we have synthesized ZnO nanorods apparently nucleated via a self-catalyzed growth mechanism. Here, we propose a growth mechanism for the ZnO nanorods, where the growth could be separated into two stages. The first stage is the growth of ZnO nuclei as stoichiometric and later it transforms to  $\text{ZnO}_x$ , through creation of oxygen vacancies [10].

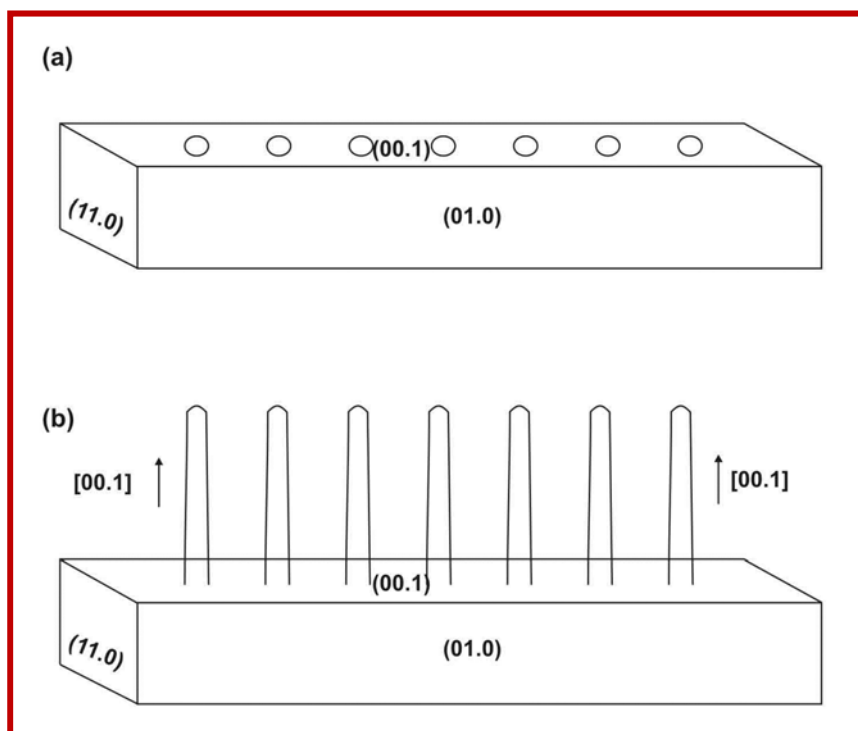
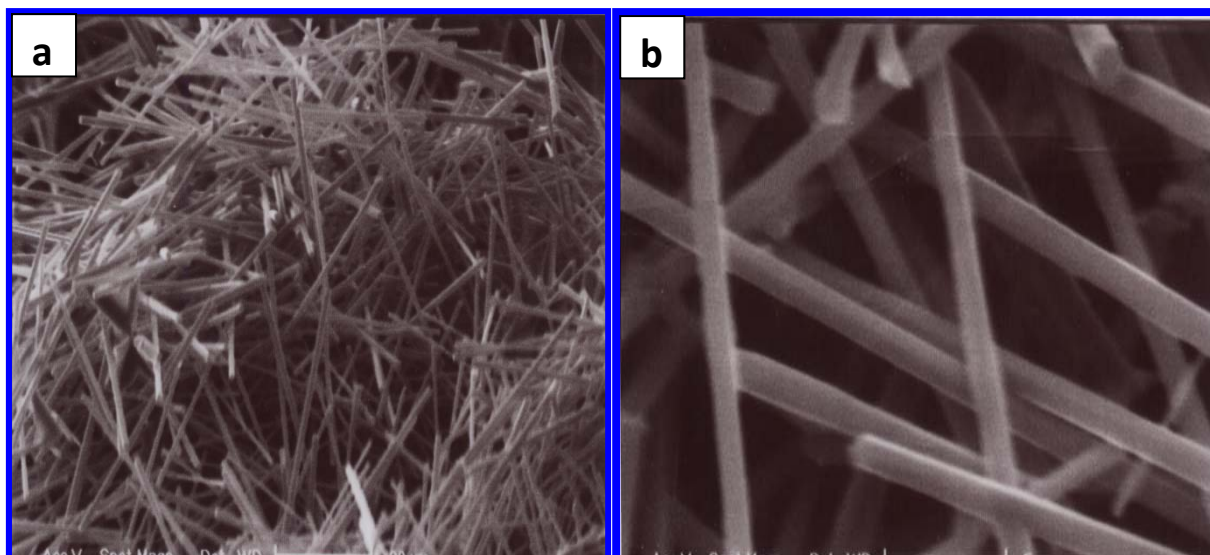


Fig. 4. Schematic diagram of the formation of ZnO nanocomb.

The second stage is the growth of  $\text{ZnO}_x$  acts as self – catalysts and leads to the formation of  $\text{ZnO}$  nanorods along  $[00.1]$  direction. By scanning tunneling microscopy, it has shown the clean  $(00.1)$  Zn faces roughen across two atomic layers in order to stabilize themselves by nonstoichiometry [25].



*Fig. 5 (a & b) low magnification SEM image of the ZnO nanorods and high magnification SEM image, respectively.*

### 3.3 Formation of ZnO nanoaeroplanes, nanotetrapods-like network

The synthesis of ZnO nanoaeroplanes and nanotetrapod-like networks was carried out in a conventional horizontal alumina tube furnace. Zinc powder (Thomas Baker 99.99% purity) was loaded in an alumina boat as source material and positioned in the hot zone of the preheated furnace and simultaneous flow of  $\text{O}_2$  [flow rate (0.5 l/m)], and Ar [flow rate (1 l/m)] ambient. ZnO nanoaeroplanes and tetrapod-like networks have also been grown successfully by varying the growth conditions. SEM and TEM images of the nanoaeroplanes are shown in figure 6. These novel structures are called nanoaeroplanes because their shapes resemble the classic triangular folded paper aeroplane. Figure 6(a) is an overall SEM image of many nanoaeroplanes with sizes ranging from 1 to 5  $\mu\text{m}$ . The typical morphology of a nanoaeroplane is shown in figure 6(b). Every nanoaeroplane is composed of three ‘wings’ having a common axis, and a ZnO nanorods with diameter of 100–200 nm extending out from the ‘nose’. Typical SEM images of the grown samples are shown in figure 7. In the low magnification SEM images shown in figures 7(a), it can be seen that these tetrapod-like networks are composed of many tangled ZnO nanotetrapods. The leg length of each nanotetrapod unit is about 1–5  $\mu\text{m}$  and the size of the central nucleus is about 100–300 nm.

The tetrapod-like nanostructures connect with each other by joining their legs together to form a ZnO network. In the growth process of the ZnO nanoaeroplane, we speculate that the tetrapod ZnO structures form first under the conditions of high  $\text{O}_2$  content and high reaction temperature [36]. As the oxidation process continues, ZnO or  $\text{ZnO}_x$  vapour is deposited on the four legs of the tetrapod structure along the easy axis  $[00.1]$ . For the different facets of a tetrapod leg, the speed of ZnO or  $\text{ZnO}_x$  deposition is not the same. The growth speed of the two facets parallel to the wing of the nanoaeroplane is the fastest possibly because these facets have more chance to absorb the ZnO or  $\text{ZnO}_x$  vapour than other facets. May be these two facets have more dislocations than other facets, which can benefit the nucleation of ZnO connecting the two tetrapod

forms. It should be noted that although these or  $\text{ZnO}_x$  vapour. Just like the tetrapod-like structures, the growth ends of the nanoaeroplane turn thinner and thinner. With the growth proceeding, the two facets parallel to the wing become bigger and bigger, and the wings of the nanoaeroplane come into being. That is to say, the growth plane of two legs of tetrapod-like  $\text{ZnO}$  nanostructure connect together gradually to form one wing of the aeroplane. Thus, the four legs of the tetrapod-like  $\text{ZnO}$  nanostructure turn into the three wings of the nanoaeroplane. Finally, all the three wings of the aeroplane form around  $[00.1]$ , and the nanoaeroplane forms in this size a joint.

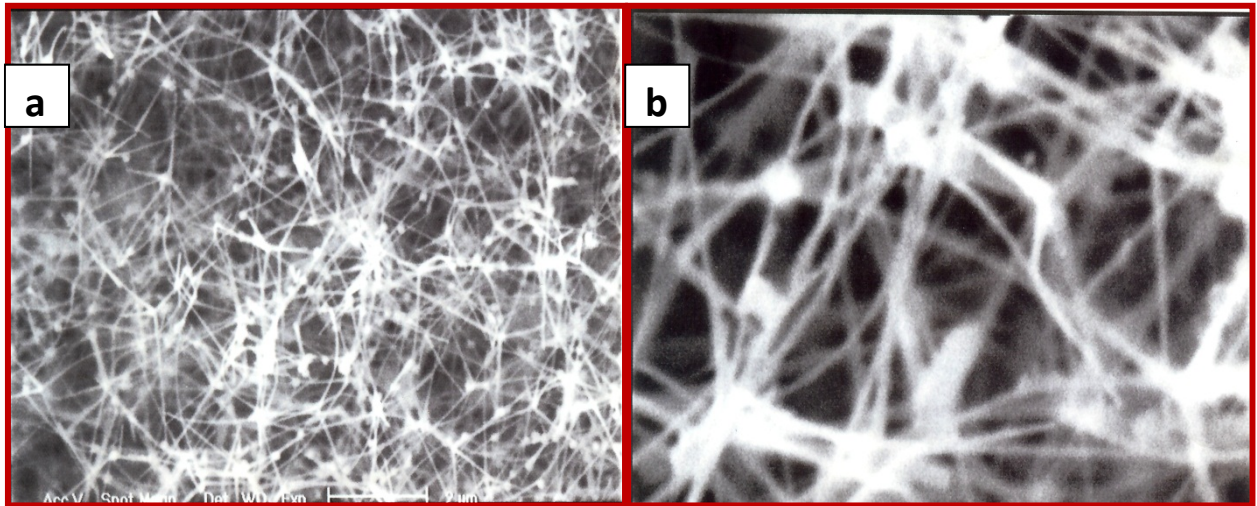


*Fig. 6 (a & b) SEM & TEM image of the ZnO nanotetrapods.*

The possible growth procedure for typical  $\text{ZnO}$  tetrapod-like networks is as follows. The  $\text{Zn}$  powder changes into  $\text{Zn}$  vapor during the evaporation period and forms  $\text{Zn}$  or  $\text{ZnO}_x$  liquid droplets as the nucleus of the  $\text{ZnO}$  networks first. Then a solid  $\text{ZnO}$  particle separates from the droplets as well as the local enrichment in  $\text{ZnO}$ , and grows along four  $[00.1]$  directions. During the growth process, the tops of the tetrapod-like unit become thinner and thinner. But when a critical size is reached, the periodic knot structure of the  $\text{ZnO}$  unit tends to come into being, possibly because the nanowire structure is the most stable structure [33]  $\text{ZnO}$  knots display periodic structures, there are small differences among them, such as diameters and lengths which can be attributed to the variation of experimental conditions (such as temperature, and the flow rate of  $\text{Ar}$  or  $\text{O}_2$ ) during the growth procedure.

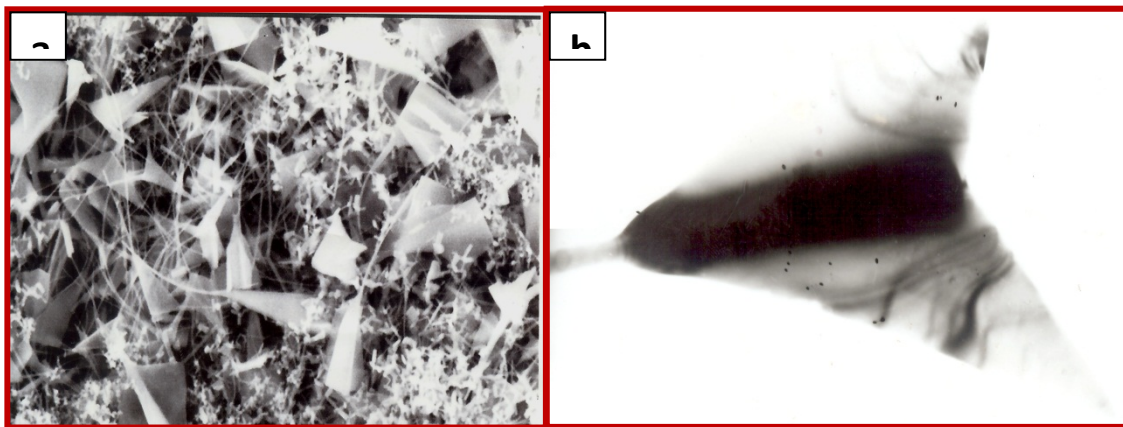


*Fig. 7(a & b) low magnification and high magnification SEM image of the ZnO nanotetrapods-like network, respectively.*

### 3.4 Photoluminescence (PL) of ZnO nanocombs

ZnO exhibits a direct band-gap of  $\sim 3.37$  eV at room temperature with large excitation energy of 60 meV. The strong exciton binding energy, which is much larger than that of GaN ( $\sim 25$  meV), and the thermal energy at room temperature ( $\sim 26$  meV) can ensure an efficient emission at room temperature under low excitation energy. As a consequence, ZnO is recognized as a promising photonic material in the blue–UV region. The light emission characteristic of the ZnO combs has been investigated by photoluminescence measurements. These have been done at room temperature employing a Perkin Elmer LS 55 luminescence spectrometer equipped with He-Cd lamp as the source of excitation and with filter 390 nm. Figure 8 shows a representative example of photoluminescence (PL) from ZnO sample, which exhibited preponderance of nanocombs like structure. As can be seen that the PL spectrum representative of nanocombs exhibits three peaks, which are located at  $\sim 380$  nm,  $\sim 428$  nm and  $\sim 500$  nm. The  $\sim 380$  nm, peak is well understood to be related to excitons emission. The broad green band at  $\sim 500$  nm, keeping in view of the known PL results from ZnO can be taken to originate from defects. However there seems to be no general agreement on the nature of defects. It has been taken to be arising due to the interstitial zinc, oxygen interstitial, oxygen vacancies, donor-acceptor complex, surface states etc. Another somewhat new feature of the PL spectrum obtained with present investigation is the appearance of weak broad and blue region emission peak at  $\sim 428$  nm (marked by arrow). The small blue peak is just adjacent to green band, most likely this has also appeared from oxygen vacancies, which may lead to different type of gap states than those oxygen vacancies, which are responsible for the green broad band emission peak. In addition, the photoluminescence of the as grown ZnO nanorod was examined at room temperature.

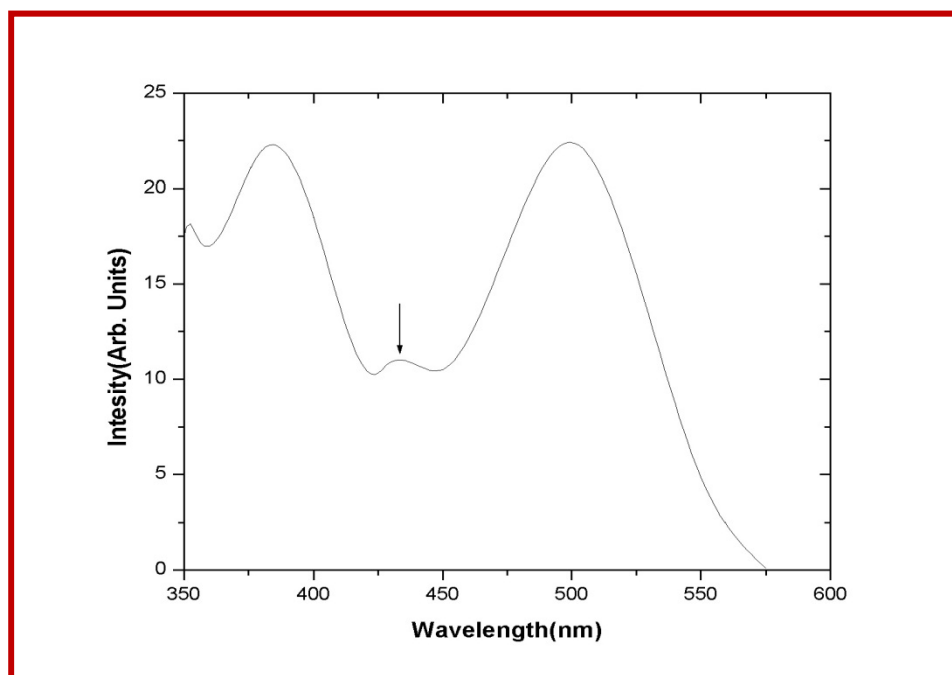


Fig. 8 Room temperature photoluminescence (PL) spectra of ZnO nanocombs .

### 3.5 Field Emission Studies of ZnO Nanocombs

The synthesized ZnO nanocomb was dispersed in methanol followed by ultrasonication for 5 minutes. A drop of the solution was taken on clean silicon flat substrate followed by drying of substrates under IR lamp for 10 minutes. These as-synthesized ZnO nanocombs coated on silicon flat substrates (0.5 cm x 0.5 cm) were used as field emitters. The field emission

measurements were carried out in an all-glass conventional field emission microscope (FEM) tube assembly consisting of an emitter cathode and a transparent anode comprising conducting coating and a phosphor layer. The FEM tube was mounted on an all-metal ultra high vacuum system comprised of an oil diffusion pump, sputter ion pump and titanium sublimation pump. The emission sites could be seen directly on the anode screen, which was held at a distance of 5 mm from the emitter cathode. After baking the tube at 250 °C for 8 hrs, pressure of  $1 \times 10^{-9}$  mbar was obtained with the help of titanium sublimation pump. The field emission current–voltage (I-V) characteristic and the current - time (I –t) records were carried out at this pressure using a Keithley 485 picoammeter and a Spellman high voltage dc power supply with proper grounding.

The electric field, (where field is defined  $E = V/d$ , where V is the applied voltage and d is the separation between cathode and anode) required to draw a current density of  $1 \mu\text{A}/\text{cm}^2$  from nanocomb, is found to be  $1.4 \text{ V}/\mu\text{m}$ . These values are comparable to those reported for various ZnO nanostructures having different morphologies and also much higher than other reports on ZnO nanocomb [16]. The total field emission current density is estimated to be  $\sim 9.05 \mu\text{A}/\text{cm}^2$  at an applied average electric field of  $\sim 1.92 \text{ V}/\mu\text{m}$  for an emitter to screen distance of 5 mm for the nanocombs.

Fig.9 (a) show the field emission current density, J as a function of the applied electric field, E (J-E plot) for ZnO combs. The inset shows (Fig.9 (b)) the corresponding Fowler-Nordheim (F-N) plots [ $\ln (J/E^2)$  vs  $(1/E)$ ] derived from the J-E characteristics. The F-N plots are seen to be nearly linear in nature in the range of applied fields, in agreement with the F-N theory [34]. The field enhancement factor  $\beta$  is directly depends on the size of the emitter tip and is estimated using the following equation,

$$\beta = (-6.8 \times 10^3 \phi^{3/2})/m \quad (3)$$

where  $\phi$  is the work function of the emitter material (in eV) and  $m$  is the slope of the F-N plot. The field enhancement factor  $\beta$  is found to be  $\sim 8050$  for the nanocomb. The high value of field enhancement factor suggests that the enhancement in the field is due to the nanometric features of the ZnO specimens. From these values, it is clear that the nanocomb is superior in field emission properties as compared to the other ZnO variants. Although the nanocombs exhibit higher value of field enhancement factor than the other ZnO nanostructures, it has a better control on the areal density of the nanorods [16-20]. The field electron emission current stability with time ( $I-t$ ) is one of the decisive requirements for practical applications. The FE current stability of ZnO nanocombs was investigated at a fixed preset value of 200 nA (Fig. 9 c) for more than 2 h duration. Initially, there is a rise in the emission current to 300 to 400 nA, and it remains nearly stable with no severe fluctuations around the average value. The fluctuations in the FE current are attributed to the adsorption and desorption of the residual gas molecules on the ZnO nanocombs emitter surface. The diffusion of the adsorbates on the emitter tip surface is also one of the possible causes of fluctuations. The observed  $I-t$  stability further emphasizes that the ZnO nanocombs exhibits good emission current stability, which can be attributed to high oxidation resistant behaviour as well as resistance of the ZnO nanocombs to ion bombardment. The FE image, recorded during the  $I-t$  measurements (Fig. 9d), displays a single bright spot. The image spot is observed to remain very stable in size and intensity over the period of operation.

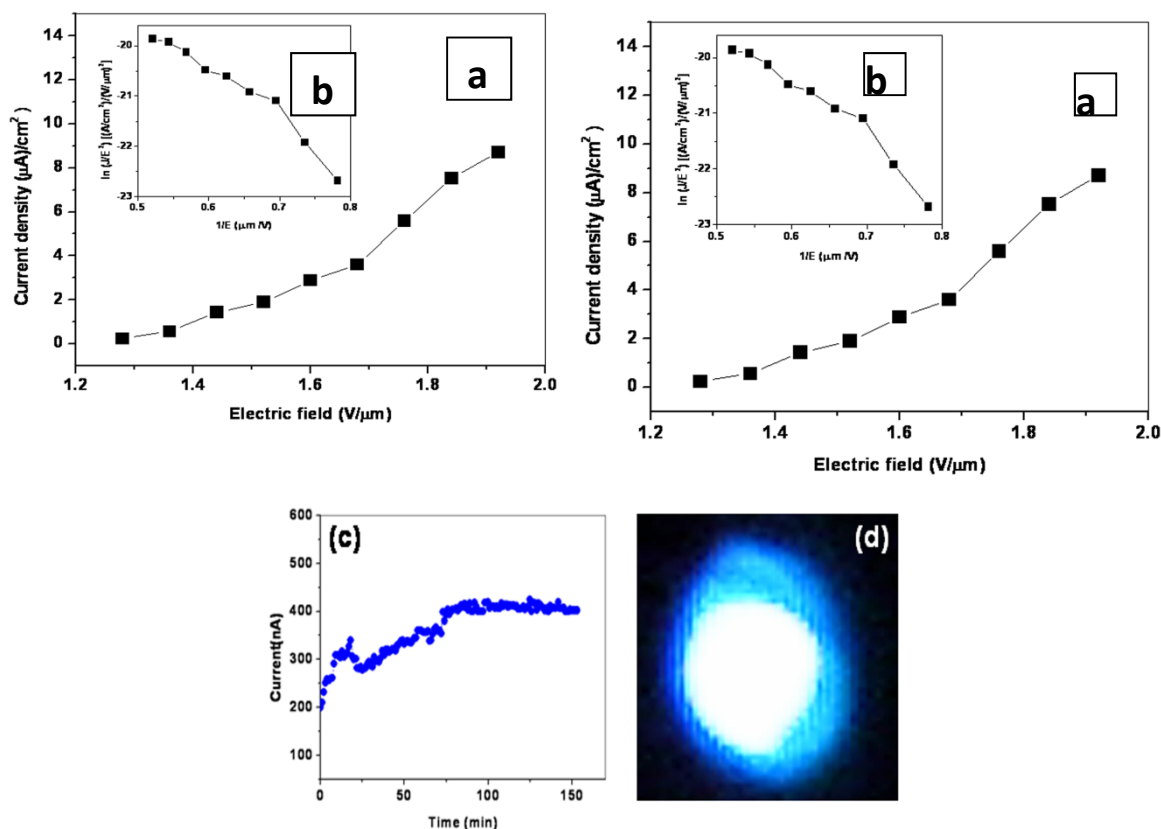


Fig. 9. Field emission from ZnO nanocombs J-E curve and (b) inset showing corresponding Fowler-Nordheim plot. (c) Field emission current stability for ZnO nanocombs and (d) shows the corresponding field emission micrographs for nanocombs.

#### 4. Conclusions

In the present investigation ZnO nanostructures with different morphologies have been fabricated by using pure zinc powder evaporation at the temperature range 400~900 °C. The morphologies of these ZnO nanostructures have been investigated by scanning electron microscopy and transmission electron microscopy. It has been found that growth parameters like temperature, gas flow rate etc. control the diameter and length of the nanorods nanocombs etc. Photoluminescence spectra and field emission property have also been measured. An emission current density of  $\sim 1 \mu\text{A}/\text{cm}^2$  has been drawn from ZnO nanorods at applied field of  $\sim 1.68 \text{ V}/\mu\text{m}$ . The field enhancement factor ( $\beta$ ) is estimated to be  $\sim 8050$  for these ZnO combs. These ZnO nanocombs and nanorods may be very attractive for commercial application as electron sources, and also have impact in applications such as optoelectrical devices, microelectromechanical system, and sensors.

#### Acknowledgments

J. Singh is thankful to the MNRE; New Delhi, India for providing financial assistance under the hydrogen mission scheme. We gratefully acknowledge the University Grant Commission (UGC), Council of Scientific and Industrial Research (CSIR) and Department of Science and Technology (DST), New Delhi for their financial support regarding this study. P. Kumar and K. Ramam also acknowledge funding support from the Fondecyt Postdoctorate Project number 3120225 and Fondecyt Regular Project number 1110583 of CONICYT-Chile, respectively. The authors are also thankful to Professor C.N.R. Rao FRS, Professor S.K. Joshi, Professor D. Chakravorty, Professor A.K. Raychaudhari for encouragement. The financial

assistance from MNRE (Jai Singh) and DST unit of Nanoscience and Nanotechnology are gratefully acknowledged. Prof. (Mrs.) S.K. Kulkarni (Pune University) is gratefully acknowledged for recording of photoluminescence properties measurement.

### References

- [1] Wang Z.L.; (ed.) Nanowires and Nanobelts – materials, properties and devices; Vol. II: Nanowires and Nanobelts of Functional Materials, Kluwer Academic Publisher, 2003.
- [2] Pan Z.W.; Mahurin S.M.; Dai S.; Lowndes D.H.; *Nano Lett.* 2005, 5, 723. doi:abs/10.1021/nl050165b
- [3] Wang Z.L.; Song J.H.; *Science* 2006, 312, 242. doi: 10.1126/science.1124005
- [4] Ozgur U.; Alivov Y.I.; Liu C.; Teke A.; Reshchikov M.A.; Dogan S.; Aurutin V.; Cho S.J. ; Morkoc H. *Appl. Phys. Rev.* 2005, 98, 043101. doi:10.1063/1.1992666
- [5] Jagdish C.; Pearton S.; Zinc Oxide Bulk; Thin Films and Nano Structures Processing; Properties and Applications; Elsevier; Oxford IX51GB UK, 2006.
- [6] Kar S.; Pal B. N.; Chaudhari S.; Chakravorty D. *J. Phys. Chem. B.* 2006, 110,4605. doi:10.1021/jp056673r
- [7] Xu C. X.; Sun X. W.; Dong Z. L.; Yu M. B. *J. Crystal Growth* 2004, 270, 498. doi:10.1016/j.jcrysgro.2004.07.010
- [8] Singh J.; Patil S. S.; More M. A.; Joag D. S. ; Tiwari R. S.; Srivastava O.N. *Appl. Surface Sci.* 2010, 256, 6157. doi:10.1016/j.apsusc.2010.03.130
- [9] Singh J.; Tiwari R. S.; Srivastava O. N. *J. Nanoscience Nanotechnol.* 2007, 7, 1783. doi: 10.1166/jnn.2007.715.
- [10] Singh J.; Srivastava A.; Tiwari R. S.; Srivastava O. N. *J. Nanoscience Nanotechnol.* 2005, 5, 2093. doi: 10.1166/jnn.2005.413.
- [11] L. Wang; X. Zhang; S. Zhao; G. Zhou; Y. Zhou ;J. Q. *Appl. Phys. Lett.* 2005, 86, 024108. doi:10.1063/1.1851607.
- [12] Lao C.S.; Gao P.X.; Yang R.S.; Zhang Y. ; Dai Y.; Wang Z. L. *Chem. Phys. Lett.* 2005, 417, 359. doi:10.1016/j.cplett.2005.10.037
- [13] Wang Z.L.; Kong X.Y.; Zuo J.M. *Phys. Rev. Lett.* 2003, 91,185502. doi: 10.1103/PhysRevLett.91.185502
- [14] Chen Y.Q.; Jiang J.; He Z.Y.; Su Y.; Cai D. ; Chen L. *Mater. Lett.* 2005, 59, 3280 . doi:10.1016/j.matlet.2005.05.059.
- [15] Manzoor U.; Kim D.K. *Scripta Mater.* 2006, 54, 807. doi: 10.4028/www.scientific.net/
- [16] Fang; Bando Y.; Gautam U. K.; Ye C.; Golberg D. *J. Mater. Chem.* 2008, 18, 509. doi: 10.1039/b712874f.
- [17] Lao, J. Y.; Huang, J. Y.; Wang, D. Z.; Ren, Z. F. *Nano Lett.* 3, 2003, 235. doi: 10.1021/nl025884u.
- [18] Lao, J. Y.; Wen, J. G.; Ren, Z. F. *Nano Lett.* 2, 2002, 1287. doi: 10.1021/nl025753t.
- [19] Wang Z.L., *Appl. Phys. A: Mater. Sci. & Processing* 88, 2007, 7, doi: 10.1007/s00339-007-3942-8
- [20] Zhuo R.F. , X. Y. Xu, H. T. Feng, D. Yan, H. J. Li, S. Cheng, Peng Xun Yan Adv. Mater. Research (Volumes 97 - 101) 960-964.
- [21] Yu X. L, Ji H M, Wang H L, Sun J, Du X.W Nanoscale Res Lett. 2010 Jan 16; 5 (3):644-648, doi:10.1007/s11671-010-9528-y.
- [22] Xiang W, Fengyu Q, Xu Z Wei C, Guozhen S *J. of Alloys and Compounds* 486, 2009, L13-L16. doi:10.1016/j.jallcom.2009.06.197
- [23] Wang Z. L., *Mater. Today*, 7, 26–33, 2004; doi.org/10.1016/S1369-7021 (04)00286-X.
- [24] T.Al-Harbi *J. of Alloys and Compounds* (2011) Volume: 509, Issue: 2, Publisher: Elsevier B.V., Pages: 387-390DOI: 10.1016/j.jallcom.2010.09.034
- [25] Zang, C.H.; Liu, Y.C.; Zhao, D.X.; Zhang, J.Y.; Shen, D.Z. *J. of Nanoscience and Nanotechnology*, Volume 10, Number 4, April 2010 , pp. 2370-2374(5).
- [26] Leung Y.H., Djurusic A.B., Gao J., Xie M.H., Wei Z.F., Xu S.J., Chan W.K., *Chem. Phys. Lett.* 394 (2004) 452
- [27] Verma A.R.; Krishna P.; Polymorphism and Polytypism in crystal; Wiley NewYork 1996.

- [28] Wander A.; Hamison N.M. *Surface Science* 2000, 468, L851. doi:10.1016/S0039-6028(00)00794-9.
- [29] J. X. Wang, X. W. Sun, and A. Wei Y. Lei, X. P. Cai, and C. M. Li Z. L. Dong *Appl. Phys. Lett.* 88, 233106; 2006. doi: 10.1063/1.2210078.
- [30] Z.H. Pan, S.M. Mahurin, S. Dai, D.H. Lowudes, *Nano. Lett.* 5 (2005) 723. doi: 10.1021/nl050165b.
- [31] C.X. Xu, X.W. Sun, Z.L. Dong and M.B. Yu. *J. Cryst. Growth*, 270 (2004), p. 498, doi.org/10.1016/j.jcrysgr.2004.07.010.
- [32] Sulieman K. M., Huang X., Liu J., Tang M. *Mater. Lett.* 61, 2007, 1756 doi:10.1016/j.matlet.2006.07.179.
- [33] Wang Z. L. *Mater. Sci. and Eng. R* 64, 2009, 33. doi:10.1016/j.mser.2009.02.001.
- [34] Fowler R. H.; Nordheim L. W. *Proc. R. Soc. London; Ser. A* 119, 1928, 173. doi: 10.1098/rspa.1928.0091.